nature communications

Article

https://doi.org/10.1038/s41467-025-64199-z

Kinetic selectivity in metal-organic framework chemical sensors

Received: 17 January 2025

Accepted: 9 September 2025

Published online: 24 September 2025

Check for updates

Aleksander Matavž[1,2] ✉, Margot F. K. Verstreken[1], Leen Boullart[1], Max L. Tietze[1], Masaya Sugihara[1], Lars Heinke[3] & Rob Ameloot[1] ✉

Selective detection of specific volatile organic compounds (VOCs) is crucial for health, safety, and environmental applications, but current sensors suffer from poor selectivity and struggle to measure specific VOCs in the presence of interfering compounds and water vapor. To address this issue, we introduce the kinetic selectivity achievable in nanoporous crystals, specifically metal-organic frameworks (MOFs), into the domain of chemical sensors. In well-selected MOFs, similar molecules can have diffusivities that differ by orders of magnitude. Measuring these diffusivity values is challenging since conventional methods based on rapid changes in atmosphere composition cannot be used in a sensing context. A temperature-perturbation method is developed for thin-film capacitive sensors with a MOF dielectric layer to enable diffusivity measurements in a fixed atmosphere. Our approach enables a single sensor to differentiate and quantify VOCs at ppm concentrations, even in mixtures containing high water vapor concentrations, outperforming a state-of-the-art ten-element sensor array.

Sensors capable of selectively monitoring specific volatile organic compounds (VOCs) would enable applications in breath-based disease diagnosis[1–3], distributed air quality measurements, checking food freshness, and monitoring exposure to toxic chemicals. In all applications, specific VOCs must be measured at ppm concentrations in the presence of other VOCs and water vapor[4]. Current sensors cannot effectively differentiate between the VOC of interest and interfering compounds[5,6].

Nature's approach to detecting VOCs, *i.e.*, olfaction, does not suffer from the same limitations. The smells we experience are triggered by VOCs binding to sensory neurons in the olfactory mucosa. In this process, both the affinity of a VOC for the mucosa and the diffusion to the receptor sites play a crucial role. While equilibrium sorption measurements have received the most attention[7–9], the importance of mass transfer is clear[10,11] since changes in diffusion rates through the mucus layer explain some periodic[10] and age-related[12] variations in olfactory sensitivity. The interplay of equilibrium and kinetic sorption characteristics determines the spatiotemporal encoding of the response pattern across the olfactory epithelium, enabling discrimination between VOCs.

To achieve more selective VOC sensors, surface coatings with well-defined adsorption sites have been used. For instance, metal-organic frameworks (MOFs), crystalline adsorbents with precisely defined pore sizes and functionalities, have been shown to capture VOCs efficiently[13–18]. Nevertheless, even though MOFs can display pronounced adsorption preferences, aiming only for a specific VOC in a complex mixture while completely avoiding interfering co-adsorption is too optimistic.

Results

Kinetic selectivity sensing

So far, sensors functionalized with MOFs or related adsorbents have exclusively relied on equilibrium adsorption to achieve selectivity. Nevertheless, in crystalline nanoporous materials, particularly those with narrow pore windows, differences in adsorption kinetics can be much more pronounced than differences in equilibrium uptake for

[1]Center for Membrane Separations, Adsorption, Catalysis, and Spectroscopy, KU Leuven Leuven, Belgium. [2]Condensed Matter Physics Department, Jožef Stefan Institute, Ljubljana, Slovenia. [3]Institute of Chemistry and Biochemistry, Freie Universität Berlin, Berlin, Germany. ✉e-mail: aleksander.matavz@ijs.si; rob.ameloot@kuleuven.be

similar adsorbates. Even molecules with comparable equilibrium uptakes can have diffusivities that differ by orders of magnitude, especially when they vary slightly in size[19]. In this work, inspired by the role of mass transfer in the olfactory mucosa, we introduce the kinetic selectivity achievable in nanoporous crystals into the domain of chemical sensors. This measurement concept paves the way for designing highly selective sensors that can be adapted to meet the demands of specific use cases.

Reliably measuring transport diffusivities in nanoporous crystals presents a significant challenge[20,21]; doing so in a sensor is even more daunting. Conventional experiments rely on monitoring the transient uptake or release from the adsorbent following a sudden change in the adsorbate concentration (*i.e.*, by moving between two points on an isotherm). In a VOC sensor surrounded by a fixed atmosphere to be analyzed, the non-equilibrium conditions required for measuring adsorption kinetics must be achieved differently. Since, for a given VOC concentration, the uptake in a nanoporous adsorbent is a function of temperature (Fig. 1a-b), a sudden temperature step also disrupts the equilibrium. For example, rapidly heating an adsorbent from T_1 to T_2 at a fixed analyte concentration p_1 triggers desorption until a new equilibrium uptake value q_2 is reached (Fig. 1c). When the temperature change is sufficiently rapid, the time constant of the desorption transient (τ_1) reflects the diffusivity of the analyte in the adsorbent at temperature T_2. For a well-defined adsorbent geometry such as a MOF thin film, diffusivity values can then be extracted by fitting the desorption transient with a suitable model. Solving Fick's equation for one-sided diffusion of the analyte out of the sensor's adsorbent layer yields

$$q(t) = q_i + \Delta q(T) \cdot \frac{8}{\pi^2} \sum_{i=0}^{\infty} \frac{1}{(2i+1)^2} \exp\left[-(2i+1)^2 \frac{\pi^2}{4} \frac{D}{l^2} t\right] \quad (1)$$

with q_i the initially adsorbed amount, $\Delta q(T)$ the total amount desorbed (the difference between the equilibrium uptakes q_1 and q_2 at T_1 and T_2, respectively), D the diffusivity of the analyte in the adsorbent at T_2, and l the film thickness[22,23].

To transduce the temperature-triggered desorption transient into an electrical signal, we propose a thin-film capacitor with a MOF dielectric layer and an ultra-thin, gas-permeable top electrode (Fig. 1d)[24]. This metal-insulator-metal (MIM) configuration enables high sensitivity due to the exclusion of parasitic substrate contributions to the measured capacitance[25]. At the low VOC concentrations relevant for sensing, the capacitance measured at equilibrium is linearly proportional to the adsorbed quantity of an analyte, regardless of the VOC

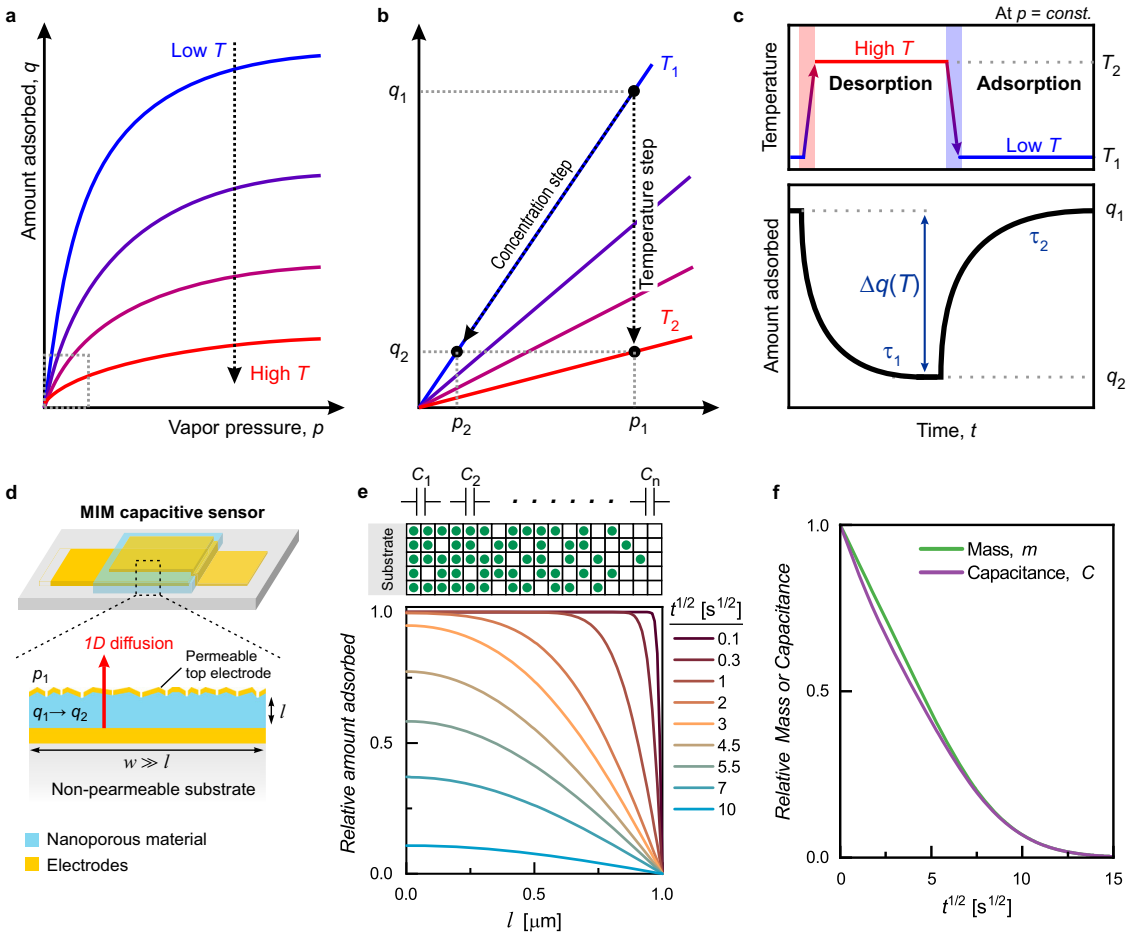

Fig. 1 | Thermal perturbation of the adsorption equilibrium and transient capacitive measurement. a Illustration of the temperature dependence of adsorption isotherms. **b** Zoom-in on the low-concentration isotherm region most relevant for sensing. The arrows indicate two ways to transition between equilibrium states with adsorbed amounts q_1 and q_2. **c** Perturbation of the adsorption equilibrium by a sudden temperature step triggers desorption upon heating and adsorption upon cooling. While the change $\Delta q(T)$ is equal for the heating and cooling steps, τ_2 is longer than τ_1 because diffusion is thermally activated. **d** Schematic representation of a thin-film capacitor featuring a nanoporous dielectric layer and a gas-permeable top electrode *with* l film thickness and w film width. **e** Simulated adsorbate distribution profiles in a nanoporous film with an arbitrary thickness of 1 μm at different time points after initiating desorption. The top part illustrates individual capacitance contributions by adsorbate (full green circles). **f** Comparison of normalized mass and capacitance transients during desorption. The capacitance measured at equilibrium is approximately proportional to the adsorbed quantity. The largest divergence occurs at $t^{1/2} \sim 3\ s^{1/2}$, when the adsorbate distribution is the most inhomogeneous (*cf.* panel **e**).

https://doi.org/10.1038/s41467-025-64199-z

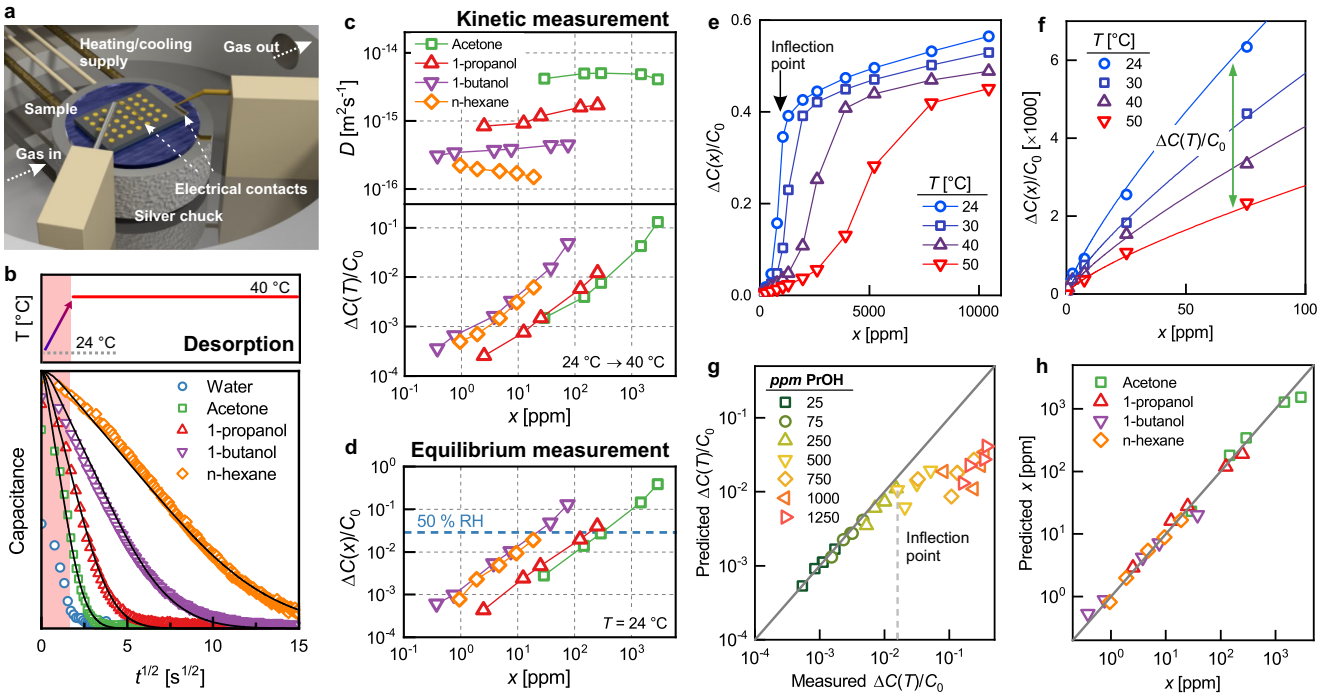

Fig. 2 | Single-analyte measurements. a Schematic representation of the measurement setup. **b** Normalized capacitance transients measured for various analytes upon thermally induced desorption. The red-shaded time window indicates the response time of the heater. For fast-diffusing compounds, such as water, most of the capacitance transient occurs within this time window, and accurate diffusivity values cannot be extracted. The black lines represent the fits to Eq. 1. **c** Kinetic selectivity sensing outputs obtained by fitting the transient sensor signal with Eq. 1: (top) diffusivity values at 40 °C and (bottom) capacitance change upon the temperature perturbation. $\Delta C(T)$ is the measured capacitance change upon heating the sensor from 24 to 40 °C at the indicated analyte concentration. C_0 is the capacitance of the sensor with a fully activated ZIF-8 layer measured at 24 °C. **d** Equilibrium response to VOCs at different low concentrations. $\Delta C(x)$ is the capacitance change upon exposing the sensor at 24 °C to the indicated analyte concentration. C_0 is the same as in panel (**c**). **e** Equilibrium capacitance as a function of 1-propanol concentration and sensor temperature. **f** Zoom-in at the low concentrations in panel (**e**). Because the isotherms diverge, the measured capacitance amplitude (green arrow) is concentration-dependent. The lines represent the fits to a Freundlich isotherm equation. **g**, Predicted and measured $\Delta C(T)/C_0$ values for 1-propanol at different concentrations and temperature steps. The four data points for each concentration correspond to $\Delta C(T)/C_0$ values predicted and measured for different temperature steps: 24 to 40 °C, 24 to 30 °C, 30 to 50 °C, and 50 to 22 °C. The response is predicted well for low concentrations, up to the isotherm inflection point. **h** Predicted and applied concentrations for a series of model VOCs for a temperature step of 24 to 40 °C. In all panels, the lines between the data points are shown to guide the eye, except in panels (**b**, **f**), where the lines are fits.

dielectric constant (SI Figure S1). To illustrate that this relationship holds during out-of-equilibrium measurements, *i.e.*, when the adsorbate distribution is non-uniform over the thickness of the adsorbent film, the response of an equivalent circuit composed of capacitors in series was considered (Fig. 1e). These simulations reveal only a minor deviation between the capacitance and mass transients (Fig. 1f). Therefore, using Eq. 1 to fit a measured capacitance transient accurately estimates the analyte diffusivity (errors <1%) and the change in adsorbed amount (error ~5 %).

Identification and quantification of single analytes

To demonstrate MOF-based kinetic selectivity sensing, ZIF-8 was selected since this material has a high affinity for VOCs and thin film deposition strategies are well-developed[26,27]. ZIF-8 has a three-dimensional cage-and-window pore space in which the narrow window aperture controls diffusion. Moreover, because of its flexibility, ZIF-8 does not exhibit a sharp size cut-off for VOCs that can enter the pores. This is beneficial since larger molecules can still enter, yet their diffusivity strongly depends on their size and thus can be used to discriminate between VOCs.

Single-analyte sensing experiments were performed by first exposing a MIM capacitor with ultra-thin gold electrodes and a ZIF-8 dielectric layer to an analyte atmosphere and subsequently heating the sensor rapidly from 24 to 40 °C (Fig. 2). The markedly different capacitance transients illustrate the significant variation in diffusion kinetics of the adsorbates in ZIF-8, with water diffusing the fastest and hexane the slowest (Fig. 2b). For all VOCs, diffusion out of the ZIF-8 layer took longer than the time required to apply the thermal perturbation, indicated by the red-shaded time window in Fig. 2b. Using Eq. 1 to fit each transient enabled the extraction of a diffusivity value and a pre-exponential factor corresponding to the desorbed quantity, further referred to as amplitude. These diffusivities closely matched those obtained by independent concentration-step measurements using quartz crystal microgravimetry (QCM) (SI Table S1). For fast-diffusing compounds, in this case, water, the whole capacitance transient occurs during the temperature perturbation, and the time constant reflects the heating rate rather than diffusion in ZIF-8. The measured diffusivity values differed by orders of magnitude between VOCs and showed little concentration dependence in the ppm regime relevant for sensing (Fig. 2c). The observed trends are consistent with previously reported diffusion behavior of short-chain alcohols and alkanes in ZIF-8[28,29]. Therefore, acetone, 1-propanol, 1-butanol, and n-hexane could be readily differentiated using a single kinetic selectivity sensor. Current sensors, which typically output only the capacitance change at equilibrium, cannot provide selective analyte detection since all tested VOCs and water can give rise to an equally large equilibrium signal (Fig. 2d).

The concept of kinetic selectivity sensing demonstrated for ZIF-8 can be readily extended to other materials within the MOF family, such as ZIF-7. In ZIF-7, which has a similar cage-and-window structure but slightly smaller pore apertures, the diffusivities of the VOCs are up to two orders of magnitude lower than in ZIF-8 (SI Figure S2). Leveraging

https://doi.org/10.1038/s41467-025-64199-z

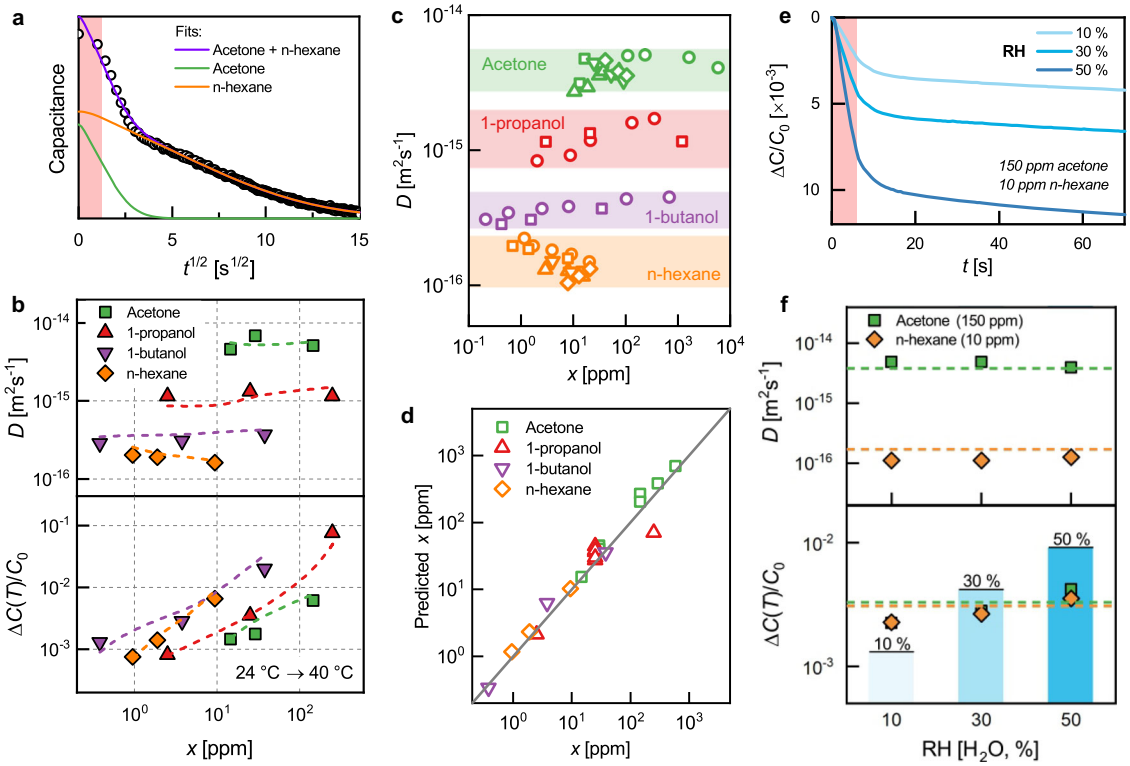

Fig. 3 | Kinetic selectivity in sensing binary and ternary mixtures. a Transient signal measured in a binary VOC mixture (150 ppm of acetone, 10 ppm of hexane) during desorption triggered by a temperature step from 24 to 40 °C. The symbols and solid lines correspond to the measured data and fits, respectively. The measured data could be accurately described as the sum of two single-analyte signals. The red band is the same as in Fig. 2b. **b** Kinetic selectivity sensing outputs obtained in binary VOC mixtures: (top) diffusivity values at 40 °C, and (bottom) capacitance change upon the temperature perturbation. The dashed lines correspond to the single-analyte data shown in Fig. 2d. The single- and multi-analyte data overlap, confirming that the VOCs diffuse independently in the MOF at these concentrations. **c** Classification of the measured analytes based on their diffusivity values. The colored bands are the 95 % confidence intervals determined based on log(*D*) values. In each band, data points from single- and multi-analyte measurements are shown together: single-analyte data (circles), binary mixture data (squares), binary mixture plus 10 % relative humidity (triangle pointing up), binary mixture plus 30 % relative humidity (triangle pointing down), binary mixture plus 50 % relative humidity (diamond). **d** Predictions of $\Delta C(T)/C_0$ for the components in binary mixtures of acetone–hexane, acetone–1-propanol, and 1-propanol–1-butanol. **e** Transient signal measured in a ternary mixture (150 ppm of acetone, 10 ppm of hexane, relative humidity ranging from 10 to 50 %) during desorption triggered by a temperature step from 24 to 40 °C. Even though adsorbed water dominates the equilibrium response, its fast diffusion out of the MOF (*cf.* initial steep drop in the transient signal) makes it possible to eliminate humidity interference via the kinetic selectivity approach. In this plot, the transient signal was not shifted (see Methods); hence, the response time is 6 s (red-shaded window). **f** Kinetic selectivity sensing outputs obtained for ternary mixtures (150 ppm acetone, 10 ppm hexane, and relative humidity levels ranging from 10 to 50 %) by fitting the same bi-exponential diffusion equation as used in panel B: (top) diffusivity values at 40 °C, and (bottom) capacitance change upon the temperature perturbation. The dashed lines indicate the values obtained in single-analyte measurements performed at the same VOC concentrations.

the diversity of MOF structures will enable shifting fast-diffusion molecules into a measurable range and promises further possibilities to improve selectivity by combining sensors based on different materials.

In addition to discriminating between VOCs, their concentrations could be quantified based on the amplitudes extracted from the capacitance transients ($\Delta C(T)/C_0$). Whereas a single isotherm describes the response of an equilibrium-based sensor, the amplitude measured by a kinetic selectivity sensor depends on the difference between the two isotherms at the initial and final temperatures of the thermal perturbation (Fig. 2e, f). Because these two isotherms diverge in the low-concentration region, the measured amplitude is concentration-dependent (Fig. 2f). Hence, once a VOC is identified, the relationship between the measured amplitude and the atmospheric concentration enables the quantification of the latter. Since this relationship is determined by the adsorption properties of the MOF layer, the sensor amplitude output can be modeled by a mathematical description of the VOC isotherm and its temperature dependence (see Methods). This approach enables the prediction of ($\Delta C(T)/C_0$ values for different temperature steps (Fig. 2g) and works irrespective of the VOC dielectric constant or polarity (Fig. 2h).

Selective detection in mixtures

Each adsorbate diffusing into or out of the MOF layer contributes to the transient sensor signal. The kinetic selectivity sensing concept is based on deconvoluting the signal contributions of VOCs that diffuse at different rates and identifying these compounds based on their characteristic diffusivities in the MOF. For this approach to work, no interactions between the diffusing molecules should occur, as this would affect their diffusivity values. In other words, the sensor signal measured in a mixed atmosphere should be the sum of the single-analyte signals measured at the corresponding concentrations. To illustrate that this condition is met at the low concentrations relevant for sensing, binary mixtures (acetone–hexane and 1-propanol–1-butanol) were studied. Bi-exponential fits of the desorption transients measured in these mixed atmospheres demonstrated that the signal could be described as the sum of two single-analyte signals (Fig. 3a) and yielded $\Delta C(T)/C_0$ and diffusivity values close to those obtained from single-component measurements at the same concentrations (Fig. 3b).

To further confirm that co-adsorbed VOCs diffuse independently in ZIF-8, the multi-analyte measurements were analyzed using the Maxwell-Stefan model, which describes binary mixture diffusion based

on three diffusivity terms. Two of these terms indicate the interaction of the diffusing molecules with the porous framework, and the third reflects interaction effects between the mixture components (SI Note 1, SI Table S3)[30]. When interactions between the diffusing molecules occur, the interaction term becomes smaller than the diffusivities of the individual components. In contrast, in our case, the interaction term is 500 times and 5 times larger than the slowest component in the acetone-hexane and 1-propanol–1-butanol mixtures, respectively, which indicates that the diffusion of each VOC is practically unaffected by the presence of the other component. This result can be rationalized based on the framework topology of ZIF-8, which consists of cages separated by narrow windows. The diffusion rate through the pores is determined by molecules jumping through these windows one at a time, while molecules can easily pass each other in the cages[31].

Because analytes diffuse independently of each other and their diffusivities in the MOF are practically constant at low concentrations, all tested VOCs can be differentiated and identified (Fig. 3c). Moreover, also in binary mixture measurements, VOC concentrations could be quantified based on the extracted amplitude values $\Delta C(T)/C_0$ (Fig. 3d). As expected for a multi-exponential fit, the quantification accuracy improved for larger diffusivity differences between the two components and amplitude ratios closer to one.

To explore the limits of the kinetic selectivity approach, sensing experiments were performed in humid binary VOC mixtures. These application-relevant conditions are demanding due to the much higher concentration of water compared to VOCs. In addition, for capacitive sensors, this challenge is exacerbated by the high dielectric constant of water (ε_r = 80.2 at 20 °C vs. 1.89 for hexane). For instance, despite the hydrophobic nature of ZIF-8, the small quantity of adsorbed water at 50 % relative humidity dominates the sensor's equilibrium capacitance response and drowns out the VOC signal (Fig. 3e, f). Yet, because of its small size, the diffusivity of water in ZIF-8 is at least four orders of magnitude larger than that of VOCs[32], making it possible to eliminate humidity interference via the kinetic selectivity approach. For instance, when measuring ternary mixtures of 150 ppm acetone, 10 ppm hexane, and relative humidity levels ranging from 10 to 50 %, water already fully desorbed during the temperature step (24 to 40 °C), while the VOCs needed significantly longer to reach the new equilibrium. Therefore, the resulting capacitance transient at 40 °C was nearly identical to the measurement for binary VOC mixtures in dry conditions (SI Figure S3) and could be accurately described as the sum of two single-analyte signals. Again, acetone and hexane could be identified based on the extracted diffusivities, which were nearly identical to the values obtained from single-component measurements at the same concentrations (Fig. 3f). Quantification of each VOC's concentration based on the extracted amplitude values $\Delta C(T)/C_0$ proved possible as well, albeit with small deviations compared to the single-analyte measurements at the same concentrations (Fig. 3f).

An equilibrium-based sensor, even a hypothetical perfectly selective one, cannot identify, let alone quantify, more than one analyte since all analyte contributions are lumped into a single output value. To analyze VOC mixtures and attempt to overcome the selectivity issues of current VOC sensors, multiple such elements have been arrayed together in so-called electronic noses[33]. In theory, when enough orthogonal information is present in the combined output of such a sensor array, an analyte of interest can be detected in the presence of interfering compounds. To benchmark the selectivity achievable using a single kinetic selectivity sensor, the same VOCs were analyzed using a commercial electronic nose comprising an array of ten metal oxide semiconductor sensors (**SI** Figure S4). Interestingly, even in single-analyte measurements, the electronic nose failed to differentiate acetone, 1-propanol, 1-butanol, and n-hexane (SI Figure S5). The successful differentiation of these VOCs by a single kinetic selectivity sensor, even at ppm concentrations and in mixtures containing high water vapor concentrations, illustrates the potential of the proposed approach.

In summary, we introduced the kinetic selectivity achievable in nanoporous crystals for the first time into the domain of chemical sensors. Based on a temperature-perturbation method, VOC diffusivity values could be measured in a fixed atmosphere, and a single kinetic selectivity sensor could differentiate and quantify these analytes at ppm concentrations, even in mixtures containing high water vapor concentrations, outperforming a state-of-the-art electronic nose. Harnessing the structural diversity of MOFs in kinetic selectivity sensors will enable the development of highly adaptable sensor arrays, opening the door to a wide range of VOC measurement applications that have previously been limited by the lack of selective sensors.

Methods

Transient capacitance simulations

The out-of-plane concentration gradients were calculated by assuming Fickian diffusion in a plane sheet with infinitely large lateral dimensions compared to its thickness (< 1 μm). Unobstructed diffusion from the top surface (without surface barriers) and no diffusion from the bottom surface were taken as boundary conditions. The diffusivity of the adsorbent was 10^{-14} m^2 s^{-1}. The local capacitance was calculated from the concentration profiles using effective medium approximation (Bruggeman model) and exhibited a linear relationship. The measured (macroscopic) capacitance was approximated by slicing the nanoporous film into individual layers (1000 in total) and calculating impedance by using an equivalent circuit consisting of capacitors connected in series.

Sample preparation

ZIF-8 thin films were deposited onto gold-coated silicon wafers as previously described[25,27]. The film thickness was measured using ellipsometry (Woolllam iSE). The crystallinity of the deposited materials was verified using grazing-incidence X-ray diffraction (PANalytical Empyrean equipped with a Cu-tube and a PIXcel detector). Circular gold top electrodes (12 nm thick, 0.2–1 mm in diameter) were deposited using shadow masks on an Angstrom thermal evaporator at a deposition rate of 0.5 Å/s. The measurements were performed on MIM capacitors with a 180 nm thick ZIF-8 layer and 0.4 mm diameter circular top electrodes. Samples for QCM measurements were prepared by depositing 280 nm thick ZIF-8 films on Au-coated 5 MHz AT-cut QCM sensors (AWSensors) using the same ZIF-8 film growth procedure as for the capacitive sensors.

QCM measurements were performed on an AWSensors X4 QCMD (QCM with dissipation monitoring) instrument with four custom-made high-temperature cells that can be read out in parallel. Au-coated 5 MHz AT-cut QCM sensors (AWSensors) were used. The frequency of the resonance and the bandwidth of the peak (Half-Width at Half Maximum) were recorded for the fundamental frequency, $n = 1$, and six overtones: $n = 3$, 5, 7, 9, 11, and 13. The layers were considered rigid, and the Sauerbrey equation was applied to calculate the average and 95 % confidence interval of the specific mass (m, ng cm^{-2}) of the layer[34]. All experiments were performed at 24 °C. Equilibrium isotherms were collected by exposing the sensor to a series of stepwise increasing analyte concentrations in a continuously flowing carrier gas N_2, covering a concentration range from 0.005 % p/p^0 to 60 % p/p^0. The total vapor flow was kept constant to avoid effects in the QCM signal due to pressure changes. The equilibrium amount adsorbed of the analyte was calculated from the frequency shift when the signal had stabilized. Transient uptake and release response curves were collected following the frequency shift over time when inducing a concentration shift in the measurement chamber.

Kinetic selectivity sensing measurements were performed at 100 kHz using a Keysight E4980AL LCR meter. The measurements were performed in an environmental cell with a temperature-controlled stage

(Linkam THFS600E-PB4). A gentle contact to the top electrodes was provided using a thin gold wire (50 μm) glued to the needle probe with silver paint (Leitsilber 200, Ted Pella). The thermal time constant of the setup for a typical heating step from 24 °C to 40 °C was about 6 s ($dT/dt = 2.5\ K\ s^{-1}$), which limited the fastest measurable diffusivity to 6×10^{-15} $m^2\ s^{-1}$ for a 180 nm film and to 5×10^{-14} $m^2\ s^{-1}$ for a 500 nm film (see SI Figure S6 for more details and bandwidth plots). To approximate the instant T-step in the modeling of kinetic parameters, the diffusion transients were shifted by subtracting the first 3 seconds (thermal time constant, SI Figure S7). In a typical sensing experiment, the sensor was first exposed to pure nitrogen gas until reaching a stable baseline value (C_0). A desired VOC concentration was then introduced in the environmental cell using the VOC supply unit. The kinetic measurements were performed once the sensor signal stabilized, typically by heating from 24 to 40 °C. After the new equilibrium was reached, the reversibility of desorption was evaluated by cooling the sample from 40 to 24 °C. The intrinsic capacitive thermal response of the Au/ZIF-8/Au device, $\Delta C(T)/C_0 = 6 \times 10^{-5}$ 1/K, measured separately in pure nitrogen, was found to be instantaneous and could readily be compensated for in the sensing experiments (SI Figure S8). For all VOCs, Eq. 1 was used to fit the capacitance transients and extract diffusivities and amplitudes. In the case of water, this approach was not followed because it diffuses several orders of magnitude faster in ZIF-8 than the thermal response of the heater ($D = 2 \times 10^{-11}$ $m^2\ s^{-1}$ at 40 °C, corresponding to the time constant of 5.4×10^{-4} s for 180 nm thick film)[19]. In multi-analyte measurements, the accuracy of the fit improved for larger diffusivity differences between the two components and amplitude ratios closer to one. To assess the impact of the concentration ratio, experiments with a fixed 1-propanol concentration (25 ppm) and varying acetone concentrations (30–580 ppm) were performed. Despite the small difference in diffusivities (6.6×10^{-15} $m^2\ s^{-1}$ for acetone and 1×10^{-15} $m^2\ s^{-1}$ for 1-propanol) and up to a 10-fold difference in amplitude (values for single components), the error in estimated diffusivity and $\Delta C(T)/C_0$ values remained below 20% and 15%, respectively.

VOC supply

VOC vapors were supplied using an in-house built dosing setup. The setup consisted of two mass flow controllers (MFCs, EL-FLOW Bronkhorst). The first MFC delivers a nitrogen carrier flow through a bubbler filled with an analyte to produce the saturated VOC vapor. The second MFC delivers a pure nitrogen stream to dilute the saturated vapor and adjust the vapor concentration to a desired value. The vapor concentration is defined as p/p^0, where p and p^0 are the actual and saturated vapor pressure of the analyte, respectively. For dielectric and gravimetric measurements, the bubbler was kept in a thermostatic bath at 21.0 °C, and the sample temperature was 24.0 °C. Hence, the reported p/p^0 is at 24.0 °C and was calculated according to the saturated vapor pressures at bath and sample temperature. The dosing setup reliably produces p/p^0 values between 2 and 80%. A dilution module was used for reaching lower concentrations, for which a vapor with p/p^0 = 2.5–5% was fed into the module and diluted with pure nitrogen by adjusting the gas flows through the MFCs. Binary and ternary mixtures were produced by mixing single-component vapors.

Phenomenological model for $\Delta C(T)/C_0$ prediction

The equilibrium response of ZIF-8 sensors was linear in the log-log plots (**SI** Figure S9) and can be accurately approximated by a Freundlich-like equation $R(T) = b(T) \cdot x^n$, where $R = \Delta C(x)/C_0$ is sensor response, b is the partition coefficient, and n describes the heterogeneity of adsorption ($n \leq 1$). For a fixed temperature perturbation, the amplitude can be calibrated by measuring partition coefficients at the initial and final temperatures. For real-world sensing applications, it might be desirable to maintain the initial temperature at ambient conditions (e.g., to save power). Since, in that scenario, the initial temperature might fluctuate, we propose a phenomenological model to describe the temperature dependence of the partition coefficient and account for arbitrary temperature steps:

$$b(T_2) = b(T_1) \exp\left[h\left(\frac{1}{T_2} - \frac{1}{T_1}\right)\right] \quad (2)$$

where h is a thermodynamic (fit) parameter. Two datasets are necessary to estimate the fit parameters (b, n, h) accurately: (i) dataset with varying concentration for a fixed temperature step, and (ii) dataset with varying temperature step with fixed concentration. For ZIF-8 sensors, the proposed model gives excellent agreement with the experimental amplitude values in the tested temperature range (from 22 to 50 °C).

Electronic nose benchmark measurements

The Portable Electronic Nose PEN3 from Airsense Analytics (Schwerin, Germany) was selected as a representative example of current electronic nose technology. The PEN3 unit integrates ten different metal oxide sensors operating between 350 and 500 °C. Single- and multi-analyte mixtures were provided the same way as in the kinetic selectivity sensing experiments, except that dried air (dewpoint of −40 °C) instead of nitrogen was used as a carrier gas to ensure optimal working conditions for the electronic nose. Before each measurement, purging was continued until a stable baseline was obtained for each sensing element. Dosing experiments involved consecutive concentration steps concentrations ranging from 0.2 to 209 ppm of the VOCs (15–200 ppm acetone, 1–209 ppm 1-propanol, 0.2–202 ppm 1-butanol, and 5–175 ppm n-hexane), and 5–50 %rH water. The electronic nose sampled the provided mixture at 40 ml/min. For each concentration step, an equilibration time of 15 minutes was allowed, followed by purging for at least 15 min to zero the response of the sensor elements. The measured data was processed using PLS_Toolbox (Eigenvector Research, Inc., Washington, USA) in a MATLAB environment (The MathWorks, Inc, Massachusetts, USA). The input data matrix comprised, for each of the measured 52 single-analyte samples, the responses of each of the 10 sensors as variables. As a preprocessing step, the data was mean-centered for each sensor. Venetian blinds cross-validation with a 10/90 data split was employed. The principal component analysis (PCA) model included three principal components, capturing 47.24 %, 32.61 %, and 12.44 % of the variance in the original dataset, respectively. Based on this model, 95 % confidence intervals were determined and indicated as ellipses on the scores plot.

Reporting summary

Further information on research design is available in the Nature Portfolio Reporting Summary linked to this article.

Data availability

All data generated in this study are provided in the Supplementary Information and the Source Data File. Source data are provided with this paper.

References

1. Peng, G. et al. Diagnosing lung cancer in exhaled breath using gold nanoparticles. *Nat. Nanotechnol.* **4**, 669–673 (2009).
2. Davis, C. E., Schivo, M. & Kenyon, N. J. A breath of fresh air – the potential for COVID-19 breath diagnostics. *EBioMedicine* **63**, 103183 (2021).
3. Shirasu, M. & Touhara, K. The scent of disease: volatile organic compounds of the human body related to disease and disorder. *J. Biochem.* **150**, 257–266 (2011).
4. Jia, Z., Patra, A., Kutty, V. & Venkatesan, T. Critical Review of Volatile Organic Compound Analysis in Breath and In Vitro Cell Culture for Detection of Lung Cancer. *Metabolites* **9**, 52 (2019).
5. Lewis, A. & Edwards, P. Validate personal air-pollution sensors. *Nature* **535**, 29–31 (2016).

6. Khatib, M. & Haick, H. Sensors for Volatile Organic Compounds. *ACS Nano* **16**, 7080–7115 (2022).
7. Mozell, M. M. Evidence for Sorption as a Mechanism of the Olfactory Analysis of Vapours. *Nature* **203**, 1181–1182 (1964).
8. Mozell, M. M. & Jagodowicz, M. Chromatographic Separation of Odorants by the Nose: Retention Times Measured across in vivo Olfactory Mucosa. *Science* **181**, 1247–1249 (1973).
9. Hornung, D. E., Lansing, R. D. & Mozell, M. M. Distribution of butanol molecules along bullfrog olfactory mucosa. *Nature* **254**, 617–618 (1975).
10. Nachbar, R. B. & Morton, T. H. A Gas chromatographic (GLPC) model for the sense of smell. Variation of olfactory sensitivity with conditions of stimulation. *J. Theor. Biol.* **89**, 387–407 (1981).
11. Hahn, I., Scherer, P. W. & Mozell, M. M. A Mass Transport Model of Olfaction. *J. Theor. Biol.* **167**, 115–128 (1994).
12. Shirai, T. et al. Functions of human olfactory mucus and age-dependent changes. *Sci. Rep.* **13**, 971 (2023).
13. Stassen, I. et al. Towards metal–organic framework based field effect chemical sensors: UiO-66-NH2 for nerve agent detection. *Chem. Sci.* **7**, 5827–5832 (2016).
14. Campbell, M. G., Sheberla, D., Liu, S. F., Swager, T. M. & Dinca, M. Cu3(hexaiminotriphenylene)2: An Electrically Conductive 2D Metal–Organic Framework for Chemiresistive Sensing. *Angew. Chem. Int. Ed.* **54**, 4349–4352 (2015).
15. Leidinger, M., Rieger, M., Sauerwald, T., Alépée, C. & Schütze, A. Integrated pre-concentrator gas sensor microsystem for ppb level benzene detection. *Sens. Actuators B: Chem.* **236**, 988–996 (2016).
16. Zhang, D. et al. Biomimetic synthesis of zeolitic imidazolate frameworks and their application in high performance acetone gas sensors. *Sens. Actuators B: Chem.* **302**, 127187 (2020).
17. Xu, T., Xu, P., Zheng, D., Yu, H. & Li, X. Metal–Organic Frameworks for Resonant-Gravimetric Detection of Trace-Level Xylene Molecules. *Anal. Chem.* **88**, 12234–12240 (2016).
18. Qin, P. et al. VOC Mixture Sensing with a MOF Film Sensor Array: Detection and Discrimination of Xylene Isomers and Their Ternary Blends. *ACS Sens.* **7**, 1666–1675 (2022).
19. Zhang, K. et al. Exploring the Framework Hydrophobicity and Flexibility of ZIF-8: From Biofuel Recovery to Hydrocarbon Separations. *J. Phys. Chem. Lett.* **4**, 3618–3622 (2013).
20. Verstreken, M. F. K. et al. Mind the Gap: The Role of Mass Transfer in Shaped Nanoporous Adsorbents for Carbon Dioxide Capture. *J. Am. Chem. Soc.* **146**, 23633–23648 (2024).
21. Kärger, J. et al. Diffusion in nanoporous materials with special consideration of the measurement of determining parameters (IUPAC Technical Report). *Pure Appl. Chem.* **97**, 1–89 (2025).
22. J. Crank, *The Mathematics of Diffusion* (Clarendon Press, Oxford, [Eng], 2d ed., 1975).
23. J. Kärger, D. M. Ruthven, D. N. Theodorou, *Diffusion in Nanoporous Materials* (Wiley-VCH, Weinheim, Germany, 2012).
24. Tietze, M. L. & Ameloot, R. Metal organic framework photonic and electronic device for gas sensing, WO2022238569A1 (2022).
25. Matavž, A., Verstreken, M. F. K., Smets, J., Tietze, M. L. & Ameloot, R. Comparison of Thin-Film Capacitor Geometries for the Detection of Volatile Organic Compounds Using a ZIF-8 Affinity Layer. *ACS Sens.* **8**, 3167–3173 (2023).
26. Tu, M., Wannapaiboon, S., Khaletskaya, K. & Fischer, R. A. Engineering Zeolitic-Imidazolate Framework (ZIF) Thin Film Devices for Selective Detection of Volatile Organic Compounds. *Adv. Funct. Mater.* **25**, 4470–4479 (2015).
27. Lu, G. & Hupp, J. T. Metal–Organic Frameworks as Sensors: A ZIF-8 Based Fabry–Pérot Device as a Selective Sensor for Chemical Vapors and Gases. *J. Am. Chem. Soc.* **132**, 7832–7833 (2010).
28. Chmelik, C. Characteristic features of molecular transport in MOF ZIF-8 as revealed by IR microimaging. *Microporous Mesoporous Mater.* **216**, 138–145 (2015).
29. Chmelik, C. & Kärger, J. The predictive power of classical transition state theory revealed in diffusion studies with MOF ZIF-8. *Microporous Mesoporous Mater.* **225**, 128–132 (2016).
30. Krishna, R. The Maxwell–Stefan description of mixture diffusion in nanoporous crystalline materials. *Microporous Mesoporous Mater.* **185**, 30–50 (2014).
31. Chmelik, C. et al. Mass Transfer in a Nanoscale Material Enhanced by an Opposing Flux. *Phys. Rev. Lett.* **104**, 085902 (2010).
32. D. R. Lide, *CRC Handbook of Chemistry and Physics: 2005-2006 a Ready-Reference Book of Chemical and Physical Data* (CRC press Taylor & Francis Group, Boca Raton New York Washington, 86th ed., 2005).
33. Röck, F., Barsan, N. & Weimar, U. Electronic Nose: Current Status and Future Trends. *Chem. Rev.* **108**, 705–725 (2008).
34. Reviakine, I., Johannsmann, D. & Richter, R. P. Hearing What You Cannot See and Visualizing What You Hear: Interpreting Quartz Crystal Microbalance Data from Solvated Interfaces. *Anal. Chem.* **83**, 8838–8848 (2011).

Acknowledgements

The authors acknowledge SweepMe! for computer control of electrical measurements. This work was supported by European Union's EU Framework Program for Research and Innovation Horizon Europe under ERC grant agreement n° 101045433 (R.A.), acronym: KISSIES, and MSCA grant agreement n° 101072845 (R.A.), acronym: SENNET; MSCA-PF grant agreement n° 101110882 (A.M.), acronym LibMOF; Research Foundation Flanders (FWO Vlaanderen) grant agreement n° 1S48221N (M.F.K.V.), G087422N (R.A.), G0A1B24N (R.A.), and G85720N (R.A.); VLAIO Moonshot grant agreement n° HBC.2020.2612 (R.A.), acronym MOONRISE; KU Leuven grant agreement n° C14/20/085 (RA); and ARIS research program P1-0125 (AM).

Author contributions

Conceptualization: A.M., R.A., M.F.K.V.; Data curation: A.M., R.A.; Formal analysis: A.M., M.F.K.V., M.S., L.B.; Funding acquisition: R.A.; Investigation: A.M., M.F.K.V., M.S., L.B.; Methodology: A.M., R.A., M.F.K.V., L.B., M.L.T., M.S., L.H.; Supervision: R.A.; Visualization: A.M., R.A., M.F.K.V.; Writing – original draft: A.M., R.A.; Writing – review & editing: A.M., R.A., M.F.K.V., L.B., M.L.T., M.S., L.H.

Competing interests

A.M. and R.A. are inventors on a patent application (EP23715876.1 A) submitted by KU Leuven that covers the concept of kinetic selectivity sensors. The remaining authors declare no competing interests.

Additional information

Supplementary information The online version contains supplementary material available at https://doi.org/10.1038/s41467-025-64199-z.

Correspondence and requests for materials should be addressed to Aleksander Matavž or Rob Ameloot.

Peer review information *Nature Communications* thanks Hongye Yuan, and the other, anonymous, reviewer(s) for their contribution to the peer review of this work. A peer review file is available.